Quantitative inversion of azimuthal anisotropy parameters from isotropic techniques

Peter R. Mesdag[1] and Leonardo Quevedo[1]

Abstract

Exploration and development of unconventional reservoirs, where fractures and in situ stress play a key role, calls for improved characterization workflows. In this work, we present a method for quantitative estimation of anisotropic parameters related to stress and fracture detection that makes use of standard isotropic modeling and inversion techniques in anisotropic media. Based on the Rüger reflectivity equations for horizontal transverse isotropic media, we build a set of transforms that map the elastic parameters used in prestack inversion into effective anisotropic elastic parameters. When used in isotropic forward modeling and inversion, these effective parameters accurately mimic the anisotropic reflectivity behavior of the seismic data, thus closing the loop between well-log data and seismic inversion results in the anisotropic case.

Introduction

The presence of natural fractures and in situ stress induces anisotropic seismic response that is neglected in many cases of interest for petroleum geophysics, due to its complexity and subtlety. As a result, isotropic prestack inversion has become a more widely applied methodology than its anisotropic counterpart. Nevertheless, most natural sediments, through their deposition and stress, will exhibit some degree of anisotropy, and ignoring its effects while estimating rock-physics properties may lead to biased results. In addition, for unconventional reservoirs, the characterization of fracture and stress is of central importance in making drilling decisions and reducing risks. Therefore, it is necessary to extend the isotropic inversion methodologies to take these effects into account and produce quantitative estimates of anisotropic properties, like the axis of anisotropy, usually related to fracture or stress orientation.

Anisotropy of rocks has several effects on seismic data. First, the propagation velocity of the seismic waveform is dependent on the direction in which the wave propagates through the rock. As a result, the traveltime of the reflected waves is dependent on angle and azimuth between source and receiver, causing differential time shifts in the seismic gathers. Second, anisotropy alters the seismic amplitude variation with offset (AVO) reflectivity compared to isotropic conditions. Seismic reflectivity inversion is often used to produce a quantitative interpretation of layer properties in the subsurface. Typically, in seismic reflectivity inversion all events are assumed to be perfectly aligned and the propagation effects to have been removed in processing.

In this paper, we will focus on seismic modeling and inversion and therefore focus on the effects of anisotropy on seismic reflections. Under anisotropic conditions, the number of parameters describing the reflections increases. In the case of vertical transverse isotropy (VTI), the Rüger equations contain five parameters: three isotropic elastic parameters and two Thomsen parameters. For horizontal transverse isotropy (HTI), the number of parameters increases to seven and for tilted transverse isotropy (TTI) to eight.

This has two drawbacks for seismic reflectivity inversion. First, if we ignore the anisotropic character of the reflections and use isotropic inversion we obtain biased estimates of the elastic parameters from inversion. The calibration of seismic amplitudes and wavelets changes, and inversion results are no longer calibrated to the elastic well curves. Second, the number of parameters to be resolved is greater than the degrees of freedom in seismic amplitude reflections. With regular prestack data, the seismic AVO amplitudes can at best resolve three elastic parameters — intercept, gradient, and curvature — whereas seismic inversion can resolve combinations of the elastic properties P-velocity, S-velocity, and density. Even density from seismic inversion is usually questionable because long offsets and good-quality data are needed to recover it. By adding the azimuthal dimension it is possible to resolve an additional magnitude and direction. Resolving all the anisotropy parameters from seismic reflectivity inversion is, therefore, a nonunique problem.

In practice, inversion specialists will try to ignore the problems of anisotropy and perform isotropic modeling and inversion. This is a reasonable approach if the anisotropy is not diagnostic for the reservoir, such as in conventional reservoir characterization, and if the derived parameters are not too affected by the bias induced by the anisotropy.

Fortunately, the first two inverted parameters (P-impedance and S-impedance or P-impedance and V_P/V_S) are not too heavily affected by the anisotropic conditions. This means it is often possible to get away with isotropic inversion and modeling. However, there is a real danger when trying to extract density from isotropic seismic inversion under anisotropic conditions, as the "apparent" density reflectivity will change dramatically from the isotropic case and, under certain conditions, may even reverse its polarity.

To be able to cope with the nonuniqueness of the seismic data when faced with anisotropy, the industry typically has opted to change the modeling and inversion algorithms based on a certain theoretical model of the rock. The advantage of this approach is that the number of parameters controlling the reflections can be reduced, thus stabilizing the inversion process. Two major drawbacks come to mind here. First, by assuming an underlying model for the rock, the degrees of freedom of the inversion are reduced and the solutions are limited to the selected rock model. Second, a separate inversion engine needs to be designed for every type of anisotropy. The underlying model needs to be coded at the heart of the inversion, and for every rock model, confidence in the inversion technology needs to be built before the inversion results are used to help make reservoir decisions.

In this paper, we will introduce a novel technology that will make it possible to use isotropic modeling and isotropic inversion

[1]CGG.

https://doi.org/10.1190/tle36110916.1.

under anisotropic conditions. This means that trusted prestack well tying, wavelet estimation, and inversion technology can be used to achieve quantitative measures of the layers in the subsurface, even under anisotropic conditions.

This new technology, first introduced by Mesdag (2016), is based on transforming the isotropic elastic parameters to "effective" elastic parameters for certain types of anisotropy. These effective elastic parameters, which are based on the isotropic elastic parameters and the Thomsen anisotropy parameters, will mimic the anisotropic reflections when used in isotropic modeling and inversion. Presently, this transformation to effective elastic parameters can be performed for general classes of anisotropy, such as VTI, HTI, and TTI. The transforms built contain no further assumptions as to the mechanism causing the anisotropy and are applied to well-log data so that the wells can be tied to the seismic data to derive correct wavelet amplitude and phase. The effective parameters in the wells also serve to derive low-frequency models for inversion. After inversion, based on the assumed class of anisotropy, analysis can be performed to recover the reservoir parameters of interest.

The effective elastic parameters have an analogue in the concept of elastic impedance (EI). EI was introduced by Connolly (1999) to allow the use of poststack modeling and poststack inversion on angle-stack data. The measured elastic parameters V_P, V_S, and Rho are transformed into an effective impedance that mimics the reflections in a higher angle seismic stack when using a zero-offset algorithm. With the industry's acceptance of isotropic prestack inversion, interest in EI has decreased. Here we take the next step: making it possible to quantitatively use isotropic prestack modeling and inversion in an anisotropic setting.

In the next section, examples of the transforms are given for the cases of VTI and HTI. Two examples are presented showing that the effective elastic parameters and isotropic modeling give the same results as anisotropic modeling. After isotropic inversion, the bias can be analyzed by applying a Fourier analysis on the azimuthally sectored inversion results, as outlined in the section "Post inversion analysis." This is followed by a workflow example, where a typical feasibility study is outlined using a synthetic data model. As with any seismic inversion the low frequencies are not controlled by the seismic data, and a low-frequency model needs to be postulated in the azimuthal sense. One method of doing this is shown in the final section where the azimuthal low-frequency model is updated based on the interpretation of a first-pass inversion.

The transforms

For the derivation of the elastic parameter transforms we start from the basic seismic reflectivity equation:

$$R_P(\theta) = R_0 + R_2 \sin^2\theta + R_4 \sin^2\theta \tan^2\theta, \quad (1)$$

where θ is the angle of incidence and R_0, R_2, and R_4 are the intercept, gradient, and curvature of the seismic amplitude variation with angle response.

For weak anisotropy and an isotropic half-space overlaying an anisotropic half-space, Rüger (1998) presented the coefficient R for P-wave reflectivity in the VTI case

$$R_0 = \frac{1}{2}\left[\frac{\Delta Z_P}{\bar{Z}_P}\right]$$

$$R_2 = \frac{1}{2}\left[\frac{\Delta V_P}{\bar{V}_P} - \left(\frac{2\bar{V}_S}{\bar{V}_P}\right)^2 \frac{\Delta G}{\bar{G}} + \Delta\delta\right]$$

$$R_4 = \frac{1}{2}\left[\frac{\Delta V_P}{\bar{V}_P} + \Delta\varepsilon\right]$$

and the HTI case

$$R_0 = \frac{1}{2}\frac{\Delta Z_P}{\bar{Z}_P}$$

$$R_2 = \frac{1}{2}\left[\frac{\Delta V_P}{\bar{V}_P} - \left(\frac{2\bar{V}_S}{\bar{V}_P}\right)^2 \frac{\Delta G}{\bar{G}} + \left\{\Delta\delta^{(V)} + 8\left(\frac{\bar{V}_S}{\bar{V}_P}\right)^2 \Delta\gamma\right\}\cos^2(\omega-\phi)\right]$$

$$R_4 = \frac{1}{2}\left[\frac{\Delta V_P}{\bar{V}_P} + \Delta\varepsilon^{(V)}\cos^4(\omega-\phi) + \Delta\delta^{(V)}\sin^2(\omega-\phi)\cos^2(\omega-\phi)\right].$$

In these equations, Z_P represents the P-wave impedance, V_P the isotropic P-wave velocity, V_S the isotropic S-wave velocity, and G the shear modulus. ε, δ, and γ are the Thomsen parameters. ω is the azimuth of the seismic acquisition, and ϕ is the azimuth of the symmetry axis. The overstrike $^-$ indicates an average over an interface.

Note that in the HTI equations the Thomsen parameters δ and ε have a superscript $(^V)$ as they refer to the vertical, or fast, HTI velocities. ε and δ in the VTI equations and γ in the HTI equations do not have this superscript and refer to the slow velocities. To avoid confusion, we choose reference velocities to be in the isotropy plane. This convention will result in a change of sign in γ, affecting the last term of R_2.

Now we will introduce relative Thomsen parameters:

$$\varepsilon_r = \frac{\varepsilon + 1 - \bar{\varepsilon}}{1 - \bar{\varepsilon}} \quad \delta_r = \frac{\delta + 1 - \bar{\delta}}{1 - \bar{\delta}} \quad \gamma_r = \frac{\gamma + 1 - \bar{\gamma}}{1 - \bar{\gamma}}. \quad (2)$$

In these equations, the overstrike again indicates an average, background value. As for all Thomsen parameters, $\Delta\gamma_r = \Delta\gamma$, we can replace the absolute Thomsen parameter contrasts in the VTI and HTI reflectivity equations by relative contrasts. Then, by taking the logarithm of the reflectivity equation for VTI, it becomes relatively simple to find the effective elastic parameters:

$$V_P' = \varepsilon_r V_P$$
$$V_S' = \varepsilon_r^{\frac{4K+1}{8K}} \delta_r^{\frac{1}{8K}} V_S, \quad (3)$$
$$\rho' = \frac{\rho}{\varepsilon_r}$$

where $K = (\bar{V}_S/\bar{V}_P)^2$.

For HTI, it is a little more work (Mesdag et al., 2013):

$$V_P' = \left[\delta_r^{(V)}\right]^{\cos^2(\phi-\omega)} \left(\frac{\varepsilon_r^{(V)}}{\delta_r^{(V)}}\right)^{\cos^4(\phi-\omega)} V_P$$

$$V_S' = \left(\gamma_r^{(V)}\sqrt{\delta_r^{(V)}}\right)^{\cos^2(\phi-\omega)} \left(\frac{\varepsilon_r^{(V)}}{\delta_r^{(V)}}\right)^{\frac{4K+1}{8K}\cos^4(\phi-\omega)} V_S. \quad (4)$$

$$\rho' = \left[\delta_r^{(V)}\right]^{-\cos^2(\phi-\omega)} \left(\frac{\varepsilon_r^{(V)}}{\delta_r^{(V)}}\right)^{-\cos^4(\phi-\omega)} \rho$$

In equations 3 and 4, the effective elastic parameters are denoted by a prime ′. If there is no anisotropy, the relative Thomsen parameters have the value 1, highlighting how both equations reduce to the isotropic case. The HTI equation reduces to the VTI case along the symmetry axis, where $\phi = \omega$. It is important to realize here that these effective elastic parameters are not physically measurable quantities. They are substitutions for the isotropic elastic parameters in the isotropic seismic reflectivity equations under anisotropic conditions.

To tie the wells and estimate the wavelets, these transforms are used to convert isotropic elastic parameter logs into effective elastic parameters, thus taking the effect of anisotropy on the seismic reflectivity into account. Especially for the far-offset stacks, the wavelets and well ties will be more consistent.

Synthetic examples

In this section, two examples will be shown to verify the accuracy of the effective elastic parameters. Synthetic seismic gathers will be generated using the appropriate anisotropic modeling on the one hand and isotropic modeling with effective elastic parameters on the other hand.

For the first example, Figure 1 shows the input curves and the effective parameter curves. Where the Thomsen parameters are zero the effective parameters follow the isotropic parameters. Note that the anisotropic conditions reverse the contrast for some of the interfaces. This is most obvious for the density.

Figure 2 shows the synthetic angle gathers using a 25 Hz Ricker wavelet in the plane of the anisotropy symmetry axis. The black background wiggles are calculated with the Rüger equations; the red overlay is using isotropic modeling and the effective parameters. The low-incidence angles are to the left and the high incidence angles to the right. For this set of elastic parameters and Thomsen parameters, there is no difference to be seen between the synthetics using anisotropic modeling and isotropic modeling with the effective elastic parameters.

The Rüger equation 1 defines the reflectivity at an interface between an isotropic layer overlaying an anisotropic layer. By introducing the effective elastic parameters, we have transformed the Rüger reflectivity definition into layer properties. Therefore, we are no longer limited to an interface between an isotropic and an anisotropic layer, and we are able to describe an arbitrary stack of isotropic and anisotropic layers. In the following example, we consider a four-layer medium with two HTI layers wedged between two isotropic layers. The HTI layers differ in Thomsen parameters and also in the azimuth of the anisotropy axis. Again, two methods of forward modeling are shown. First, we use isotropic modeling and effective elastic parameters and, second, anisotropic modeling using the Pšenčik and Martins (2001) anisotropic reflectivity equations.

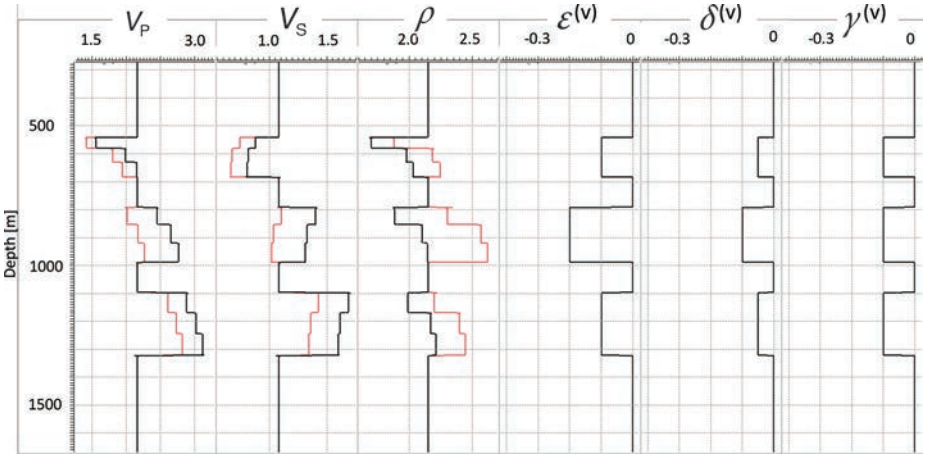

Figure 1. Well curves used for the first synthetic example. From left to right in black are the P-velocity, S-velocity, density, and the Thomsen parameters. The effective elastic parameters V_P', V_S', and r' are shown in red in the first three panels.

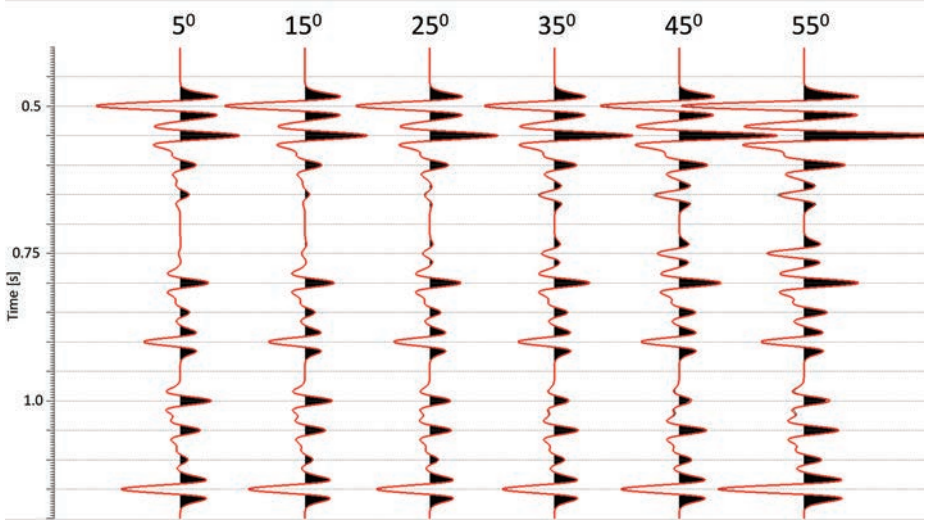

Figure 2. Synthetic HTI angle gathers along the symmetry axis. Black is using the Rüger equations for the anisotropic modeling; red is using isotropic modeling with the effective elastic parameters.

Figure 3 shows common-angle, common-azimuth sections of a single common midpoint (CMP) in the four-layer model. As with the first example, the traces range from an angle of incidence of 5° to 55° and here, additionally, they cycle through six azimuth sectors from 0° to 150°. Note the similarity of the reflections at the interface between the two anisotropic layers.

Post inversion analysis

When performing isotropic inversion in an anisotropic setting, the result of the inversion will be a set of effective elastic parameters. Where the layers are anisotropic, the inversion results are biased by this anisotropy.

In VTI media, the reflectivity response is not dependent on the azimuth, so a single prestack inversion is performed. The isotropic elastic parameters can be back-calculated knowing the Thomsen parameters and substituting this into equation 3. Since the seismic inversion is only at best resolving three elastic parameters and with VTI there are five "unknowns," it is not possible to uniquely resolve all parameters without a prior model, and reservoir characterization may need to be performed using the effective elastic parameters themselves.

In the case of HTI, separate prestack inversion is performed for several azimuth sectors. This means that the sectored inversion results need to be analyzed. In this section, the HTI analysis procedure will be explained.

Seismic inversion is typically not performed using the basic elastic parameters V_P, V_S, and ρ. The most common parameter sets for inversion are I_P, I_S, V_P/V_S, and ρ. The elastic parameter transforms for these inversion parameters follow from equation 4 and are listed here:

$$I'_P = I_P \tag{5}$$

$$I'_S = \left(\frac{\sqrt{\delta_r^{(V)}}}{\gamma_r^{(V)}}\right)^{-\cos^2(\phi-\omega)} \left(\frac{\varepsilon_r^{(V)}}{\delta_r^{(V)}}\right)^{\frac{1-4K}{8K}\cos^4(\phi-\omega)} I_S \tag{6}$$

$$\left(\frac{V_P}{V_S}\right)' = \left(\frac{\sqrt{\delta_r^{(V)}}}{\gamma_r^{(V)}}\right)^{\cos^2(\phi-\omega)} \left(\frac{\varepsilon_r^{(V)}}{\delta_r^{(V)}}\right)^{\frac{4K-1}{8K}\cos^4(\phi-\omega)} \left(\frac{V_P}{V_S}\right) \tag{7}$$

$$\rho' = \left[\delta_r^{(V)}\right]^{-\cos^2(\phi-\omega)} \left(\frac{\varepsilon_r^{(V)}}{\delta_r^{(V)}}\right)^{-\cos 4(\phi-\omega)} \rho\,. \tag{8}$$

By taking the natural logarithm of equations 6–8, these equations take on the general form of a Fourier series expansion with three coefficients:

$$A' = b_0 + b_1\cos\left[2(\phi-\omega)\right] + b_2\cos\left[4(\phi-\omega)\right]. \tag{9}$$

This was reported for seismic reflection amplitudes by Ikelle (1996) and then Sayers and Dean (2001). The coefficients b_0, b_1, and b_2 are related to the Thomsen parameters and A' represents the logarithm of the effective elastic property. This provides a direct way to estimate quantities related to anisotropy by measuring the changes in the values of the effective properties with respect to their azimuthal sectors. Note here that to be able to resolve the three Fourier components of equation 9, at least five measurements are needed. In the examples in this paper, we use six azimuth sectors.

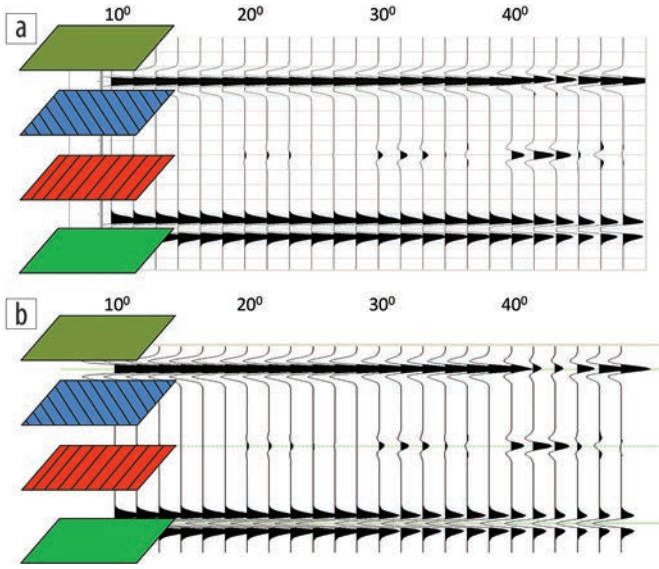

Figure 3. Full-azimuth response from the four-layer model (a) using isotropic modeling and effective elastic parameters and (b) using Pšenčik and Martins (2001) anisotropic modeling.

For V_P/V_S, the coefficients of equation 9 become:

$$\begin{aligned} b_0 &= \ln\frac{V_P}{V_S} - \frac{1}{2}\ln\gamma_r^{(V)} + \left(\frac{4K+3}{64K}\right)\ln\delta_r^{(V)} + \left(\frac{12K-3}{64K}\right)\ln\varepsilon_r^{(V)} \\ b_1 &= -\frac{1}{2}\ln\gamma_r^{(V)} + \left(\frac{1}{16K}\right)\ln\delta_r^{(V)} + \left(\frac{4K-1}{16K}\right)\ln\varepsilon_r^{(V)} \\ b_2 &= -\left(\frac{4K-1}{64K}\right)\ln\delta_r^{(V)} + \left(\frac{4K-1}{64K}\right)\ln\varepsilon_r^{(V)} \end{aligned}\,. \tag{10}$$

For effective S-impedance, the coefficients follow:

$$\begin{aligned} b_0 &= \ln I_S + \frac{1}{2}\ln\gamma_r^{(V)} - \left(\frac{4K+3}{64K}\right)\ln\delta_r^{(V)} - \left(\frac{12K-3}{64K}\right)\ln\varepsilon_r^{(V)} \\ b_1 &= \frac{1}{2}\ln\gamma_r^{(V)} - \left(\frac{1}{16K}\right)\ln\delta_r^{(V)} - \left(\frac{4K-1}{16K}\right)\ln\varepsilon_r^{(V)} \\ b_2 &= \left(\frac{4K-1}{64K}\right)\ln\delta_r^{(V)} - \left(\frac{4K-1}{64K}\right)\ln\varepsilon_r^{(V)} \end{aligned}\,. \tag{11}$$

And for effective density:

$$\begin{aligned} b_0 &= \ln\rho - \left(\frac{1}{8}\right)\ln\delta_r^{(V)} - \left(\frac{3}{8}\right)\ln\varepsilon_r^{(V)} \\ b_1 &= -\left(\frac{1}{2}\right)\ln\varepsilon_r^{(V)} \\ b_2 &= \left(\frac{1}{8}\right)\ln\delta_r^{(V)} - \left(\frac{1}{8}\right)\ln\varepsilon_r^{(V)} \end{aligned}\,. \tag{12}$$

The coefficients b_0, b_1, and b_2 can be derived from azimuthally sectored inversions by Fourier fitting to the natural logarithm of the inversions. The coefficient b_1 represents the first-order magnitude of the anisotropy, and the phase of this Fourier coefficient defines the azimuth of the anisotropy.

Workflow example

In the following sections, we go through a forward modeling and inversion workflow and show how to use effective elastic parameters in a feasibility study. Here, a synthetic data set is used, so we are able to directly compare the results with the input models. The steps are shown in Figure 4.

Of course, a synthetic case is not the full story. For a real-data example we refer to a paper by Zhang and Mesdag (2016), where this technology is applied on the Marcellus shale, and it is shown that anisotropy is not necessarily confined to single layers but may leak into the adjacent strata under strong flexing conditions. In another paper, Filipova et al. (2016) compare anisotropic inversion results with auxiliary stress measurements and microseismic events.

We first make a notional model of the HTI anisotropic subsurface defined in isotropic elastic parameters, the three Thomsen parameters and the anisotropy axis orientation. In this model, there are three different HTI layers embedded in an isotropic background model, each layer built using different HTI modeling. The top anisotropic layer follows the Hudson dry crack model (Hudson, 1980) and falls within the linear slip theory (LST), (Bakulin et al., 2000). The bottom anisotropic layer follows LST, and the middle anisotropic layer, directly on top of the bottom anisotropic layer, does not follow any fracture model.

An inversion parameterization of I_P, V_P/V_S, and density will be used here. The relationships defined in the previous section allow us to directly calculate from the model what we expect to come out of our inversion in terms of V_P/V_S and density anisotropy. In Figure 5, the expected outcomes for b_1 and b_2 are shown for V_P/V_S (equation 10) and for density (equation 11). Please note the following features in this model:

- For both V_P/V_S and density the second Fourier coefficient (b_2) is significantly smaller than the first (b_1). The Thomsen ε and δ for these models are of the same order of magnitude and largely cancel each other out in the second Fourier coefficient (b_2). For the Hudson dry cracks, they cancel out completely. This feature is important for the way we update the azimuthal low-frequency model in the final sections of this paper.
- b_1 for V_P/V_S is generally negative and b_1 for density is positive. This means that the effective V_P/V_S is highest in the isotropic plane and lowest in the direction of the anisotropy axis, while the effective density is lowest in the isotropic plane. This is important to know for the analysis of the inversion results owing to the seismic ambiguity of anisotropy magnitude and azimuth. In most cases, a negative V_P/V_S anisotropy is a correct assumption. It is not, however, a general rule, as we can see here, given that the lower anisotropy layer has a positive b_1.
- For the fracture models of Hudson and LST, the V_P/V_S anisotropy is small compared to the density anisotropy. For the chosen parameterization, the V_P/V_S anisotropy is smaller than 0.5%, while the density anisotropy is up to 10 times larger. For the analysis of anisotropy, this has two consequences. First, it will be hard to estimate the V_P/V_S anisotropy in the presence of noise. Second, the anisotropy will be mainly visible on the far offsets, putting severe constraints on the acquisition and processing of the seismic data in a real case.

In a second step, we calculate the azimuthally oriented effective elastic parameters as described in equations 7 and 8. Here, we define six equal sectors between 0° and 180°. As the anisotropic variations in the elastic parameters are only a fraction of the actual isotropic values, the azimuthally sectored effective parameters are not shown here.

The azimuthally sectored effective parameters can be analyzed on a sample-by-sample basis taking the Fourier transform in the

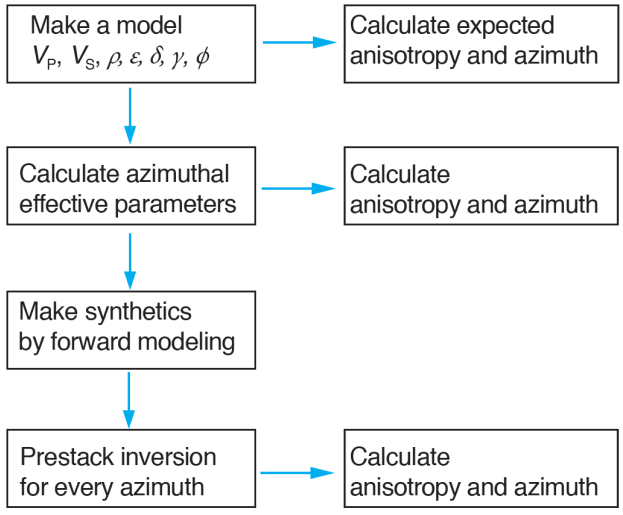

Figure 4. Workflow of an anisotropic inversion feasibility study.

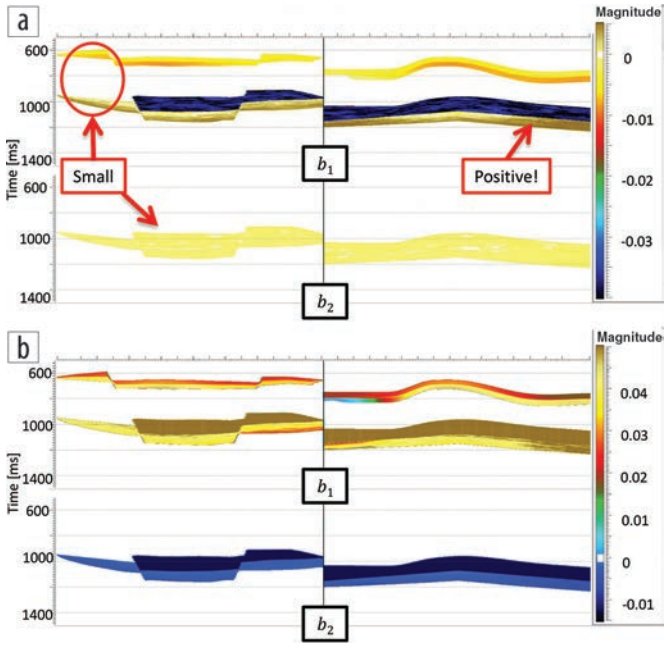

Figure 5. (a) The expected V_P/V_S and (b) density anisotropy, given the isotropic elastic parameters and Thomsen parameters of the model.

azimuthal direction. This gives us new estimates of the b_1 and b_2 of the anisotropy together with an estimate of the anisotropy azimuth, shown in Figure 6, which can be compared with the expected anisotropy in Figure 5.

Seismic data cannot resolve whether the anisotropy has one sign and a particular azimuth or whether it has the opposite sign and an azimuth rotated by 90°. Therefore, to calculate the results shown in Figure 6, we have had to predefine the sign of the anisotropy magnitude. In keeping with our general belief, we gave the V_P/V_S anisotropy a negative sign and the density anisotropy a positive sign. Where we chose the sign incorrectly, in the lower anisotropy layer, there is a 90° rotation in the anisotropy azimuth of V_P/V_S.

The next step in the feasibility workflow is the calculation of the azimuthally oriented prestack or partial stack seismic data. This forward modeling can be done either by using the initial model and anisotropic forward modeling or by using the azimuthally oriented effective parameters and isotropic forward modeling. As shown in the earlier synthetic examples, these two alternatives give exactly the same seismic synthetics. Given that the model contains stacked anisotropic layers, we would have to use the Pšenčik and Martins flavor of anisotropic reflectivity modeling. As we already had the azimuthally sectored effective elastic parameters, we used these here in an isotropic synthetic tool.

Although we have the freedom to use any wavelet in the modeling, we chose to use a simple 25 Hz Ricker wavelet. We generated six partial angle stacks ranging from 0° to 55°. No noise was added to the synthetic seismic data.

Figure 7 shows detail of two events in the synthetic seismic data. On the left-hand side, we see three seismic CMPs in a common-angle, common-azimuth plot, where the extractions are from the base of the upper anisotropic layer. As discussed earlier, this layer is dominated by density anisotropy. On the right-hand side, we see a similar plot, but now the extraction is from the top of the second anisotropic layer. This layer shows a mix of both V_P/V_S and density anisotropy. As mentioned earlier, the left-hand plot shows its main azimuthal variations on the far angles, while the azimuthal amplitude variations on the right-hand plot are more equally distributed over the angles.

The final step in the workflow is to invert every azimuth separately with an (isotropic) prestack inversion program. The inverted full-bandwidth V_P/V_S and density per azimuth are then input to the Fourier analysis to yield estimates of b_0, b_1, and b_2 and the anisotropy symmetry axis orientation after inversion. The results are shown in Figure 8 and can be compared with the expected Figure 6. Inversion has introduced a higher level of noise, which means the low values of the Fourier coefficients become invisible, but where the coefficients exceed about 2% we see good agreement, including the 90° ambiguity in the azimuth estimate in the V_P/V_S of the lower anisotropic layer. We also see that we are correctly reconstructing the azimuth, at the position where the second anisotropic layer contains an interface where only the azimuth changes, as seen on the right-hand side of the lower panels. This feature would not have been reconstructed if we had used Rüger modeling for the synthetics.

Updating the azimuthal low-frequency model

In the azimuthally sectored inversions of the previous section the appropriate effective parameter trend for each of the azimuthal sectors was used. This means that the low-frequency models varied per sector. In practice, it is not possible to do this correctly in a first-pass inversion. The Thomsen parameters and the azimuth of the anisotropy may be known at selected wells, but only guesswork is possible away from well control. Therefore, in practice, in a first iteration, the same trend will be used for every seismic sector. This single trend will most likely be derived by interpolating the isotropic well logs.

The azimuthally sectored inversions were repeated using the same isotropic trend for every sector. After choosing a negative branch for V_P/V_S in the Fourier analysis, the results are shown in

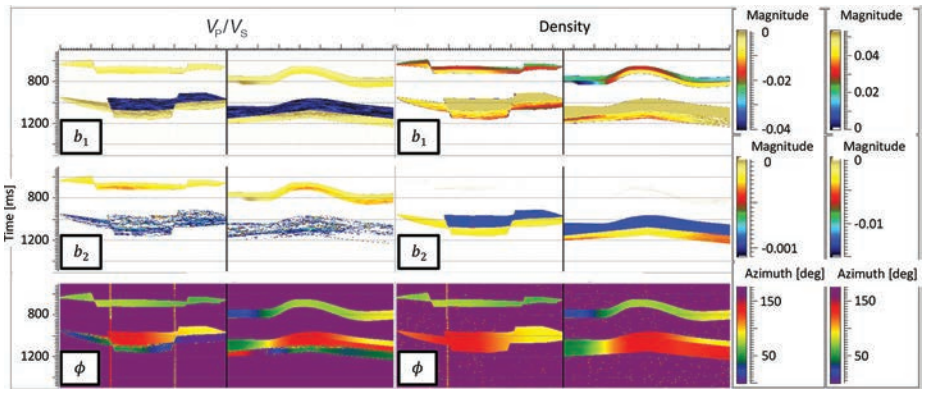

Figure 6. Anisotropy and azimuth estimates from azimuthally sectored effective V_P/V_S and density.

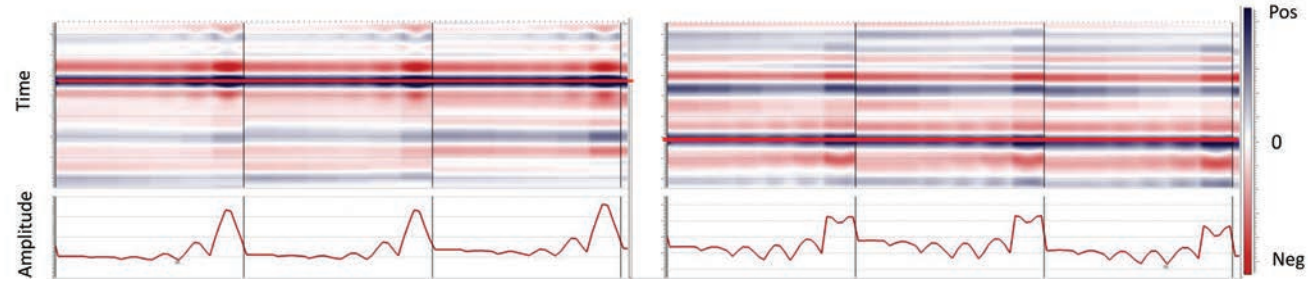

Figure 7. Details of synthetic seismic traces at three adjacent CMPs together with amplitude extractions.

Figure 9. Although the individual sectored inversions are full band, the trend is not varying in the azimuthal sense and the low frequencies are missing in the anisotropy estimates. The azimuthal information from this first-pass inversion is fundamentally band limited and the anisotropy only shows up at the interfaces where the anisotropy changes. Also the azimuth shows horizon-concurrent banding due to the 90° rotation that occurs in the sidelobes of the band-limited signal.

By extracting the azimuth directly below the top horizon and directly above the bottom horizon, we obtain two azimuth maps to be used to construct a prior azimuth model for a second-pass Fourier analysis. Instead of choosing a negative branch for V_P/V_S and getting only negative anisotropy numbers, employing a prior azimuth leads to a two-sided signal for the Fourier coefficient b_1. Since this anisotropy signal is a calibrated band-limited representation of the full bandwidth b_1, it can be used to reconstruct the full-bandwidth signal from its peak-to-trough amplitudes which correspond to relative contrasts (Mesdag et al., 2010, 2015). Such contrast in azimuth and b_1 are enough to build an azimuthal low-frequency model using the following approximation (Zhang and Mesdag, 2016):

$$\left(\frac{V_P}{V_S}\right)' \approx e^{2b_1*\cos^2(\omega-\phi)} \bullet \frac{V_P}{V_S}. \quad (13)$$

The full-band V_P/V_S data thus obtained contains enough information for a quantitative estimation of the anisotropic parameters shown in Figure 10. These estimates for azimuth and b_1 can now be quantitatively compared with the expected values in Figure 5.

Conclusions

In this paper, we introduce elastic parameter transforms that allow us to perform seismic forward modeling and inversion

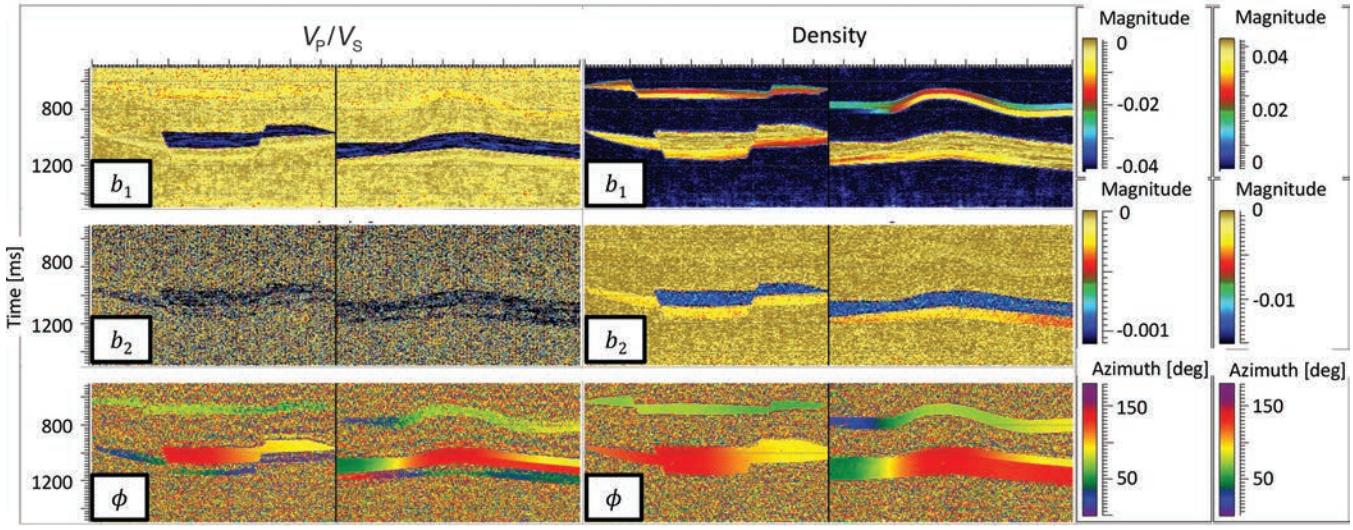

Figure 8. Anisotropy and azimuth estimates from inversion of azimuthally sectored seismic gathers.

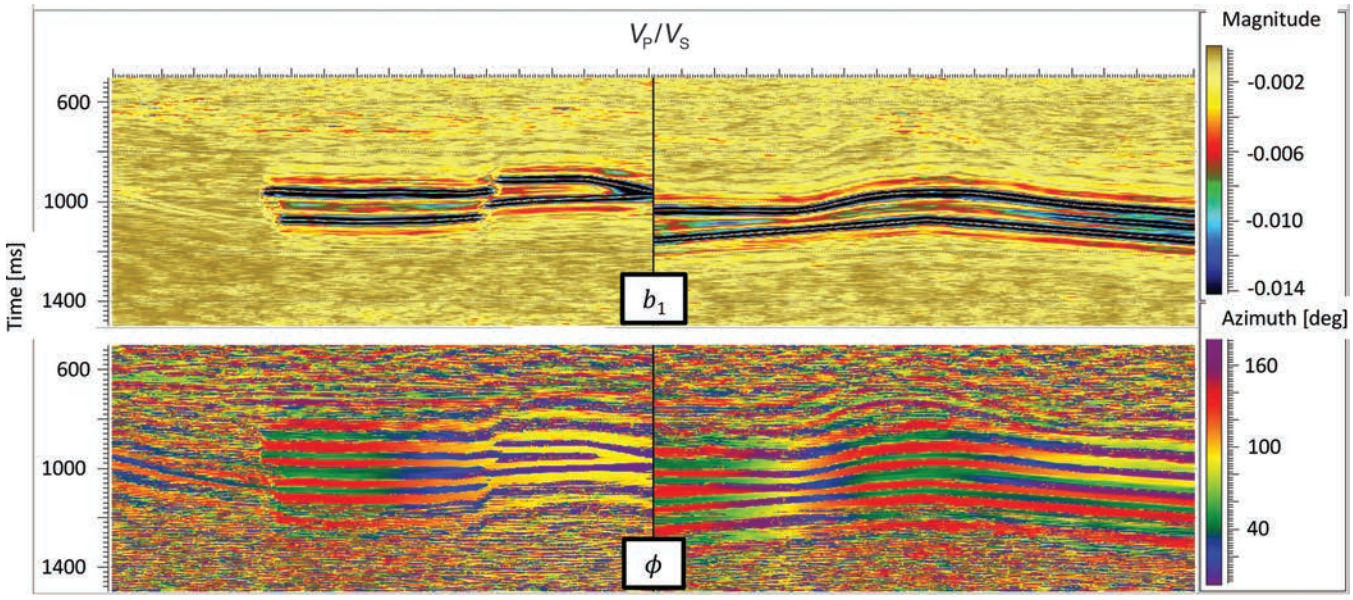

Figure 9. Anisotropy and azimuth estimates from inversion of azimuthally sectored seismic gathers, using a single isotropic background trend.

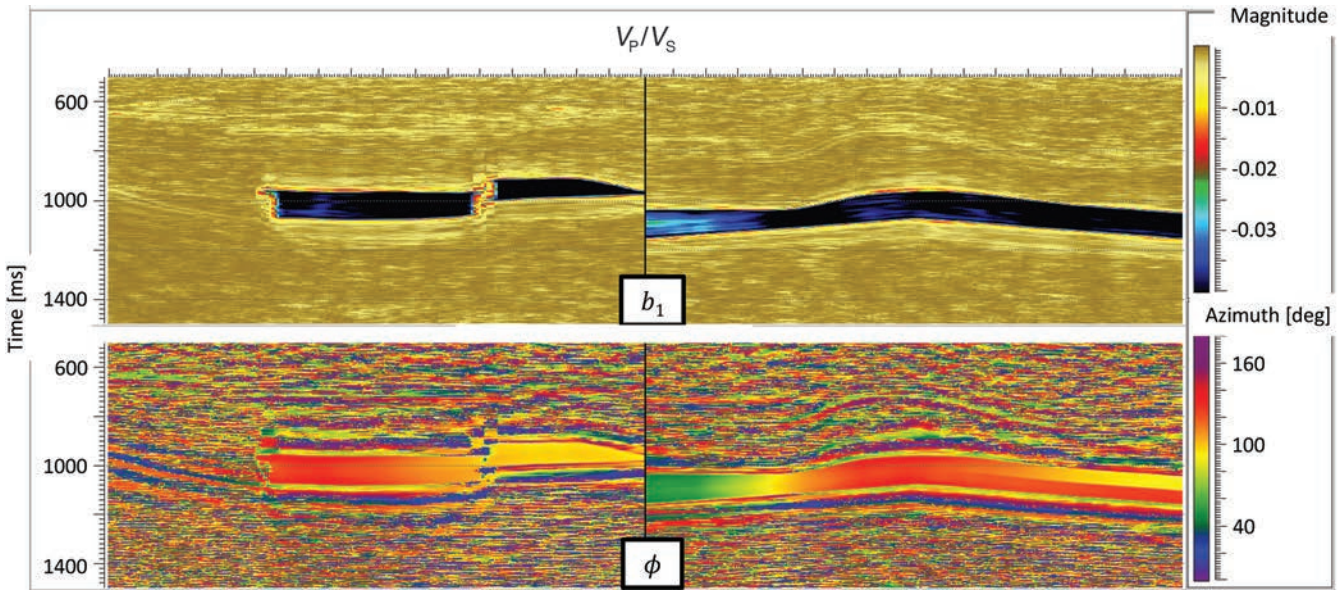

Figure 10. Anisotropy and azimuth estimates from inversion of azimuthally sectored seismic gathers, using an anisotropic background trend.

using isotropic formulations in anisotropic media. Using several synthetic examples, it is shown that the transforms are accurate for arbitrary stacks of isotropic and anisotropic layers. Effective elastic parameters are used to tie wells and estimate wavelets. No modifications are necessary to the forward modeling and inversion algorithms. Seismic inversion results are analyzed using the same elastic parameter transforms. The azimuthal variations in the signal coming out of seismic inversion of azimuthally sectored gathers are fundamentally band limited, and a method is outlined to update the low frequencies in the azimuthal sense.

The workflow introduced has been applied to a generic HTI model without suggesting any particular rock-physics model to describe the origin of the anisotropy. If such modeling is introduced, the Fourier coefficient equations (equations 10–12) particularize to simple functions of the model parameters. As an example, for the Hudson penny-shaped crack model, the Fourier coefficients are proportional to the crack density, and the azimuth exactly corresponds to the orientation of the cracks. TLE

Corresponding author: peter.mesdag@cgg.com

References

Bakulin, A., V. Grechka, and I. Tsvankin, 2000, Estimation of fracture parameters from reflection seismic data — Part I: HTI model due to a single fracture set: Geophysics, **65**, no. 6, 1788–1802, https://doi.org/10.1190/1.1444863.

Connolly, P., 1999, Elastic impedance: The Leading Edge, **18**, no. 4, 438–452, https://doi.org/10.1190/1.1438307.

Filippova, K., I. Yakovleva, P. R. Mesdag, and Y. Pavlovskiy, 2016, Stress identification with an azimuthal inversion technique — A case study for a clastic oil field: 86th Annual International Meeting, SEG, Expanded Abstracts, 2801–2805, https://doi.org/10.1190/segam2016-13868489.1.

Hudson, J. A., 1980, Overall properties of a cracked solid: Mathematical Proceedings of the Cambridge Philosophical Society, **88**, no. 2, 371–384, https://doi.org/10.1017/S0305004100057674.

Ikelle, L. T., 1996, Amplitude variations with azimuths (AVAZ) inversion based on linearized inversion of common azimuthal sections, *in* E. Fjaer, R. Holt, and J. S. Rathore, eds., Seismic anisotropy: SEG, 601–644, https://doi.org/10.1190/1.9781560802693.ch19.

Mesdag, P. R., D. Marquez, L. de Groot, and V. Aubin, 2010, Updating low frequency model: 72nd Annual Conference and Exhibition, EAGE, Extended Abstracts, https://doi.org/10.3997/2214-4609.201400777.

Mesdag, P. R., H. J. W. Debeye, and R. Bornard, 2013, Method and device for the generation and application of anisotropic elastic parameters in HTI media: PCT application WO2015/014762.

Mesdag, P. R., M. R. Saberi, and C. Mangat, 2015, Updating the low-frequency model in time-lapse seismic inversion: A case study from a heavy-oil steam-injection project: The Leading Edge, **34**, no. 12, 1456–1461, https://doi.org/10.1190/tle34121456.1.

Mesdag, P. R., 2016, A new approach to quantitative azimuthal inversion for stress and fracture detection: 86th Annual International Meeting, SEG, Expanded Abstracts, 357–361, https://doi.org/10.1190/segam2016-13684594.1.

Pšenčik, I., and J. L. Martins, 2001, Properties of weak contrast PP reflection/transmission coefficients for weakly anisotropic elastic media: Studia Geophysica et Geodaetica, **45**, no. 2, 176–199, https://doi.org/10.1023/A:1021868328668.

Rüger, A., 1998, Variation of P-wave reflectivity with offset and azimuth in anisotropic media: Geophysics, **63**, no. 3, 935–947, https://doi.org/10.1190/1.1444405.

Sayers, C., and S. Dean, 2001, Azimuth-dependent AVO in reservoirs containing non-orthogonal fracture sets: Geophysical Prospecting, **49**, no. 1, 100–106, https://doi.org/10.1046/j.1365-2478.2001.00236.x.

Zhang, M., and P. R. Mesdag, 2016, Full data-driven azimuthal inversion for anisotropy characterization: 86th Annual International Meeting, SEG, Expanded Abstracts, 403–407, https://doi.org/10.1190/segam2016-13688732.1.